Electron-impact ionization of H_2O at low projectile energy: Internormalized triple-differential cross sections in three-dimensional kinematics

Xueguang Ren,[1] Sadek Amami,[2] Khokon Hossen,[1] Esam Ali,[2] ChuanGang Ning,[3] James Colgan,[4] Don Madison,[2] and Alexander Dorn[1]

[1]*Max-Planck-Institut für Kernphysik, 69117 Heidelberg, Germany*

[2]*Physics Department, Missouri University of Science and Technology, Rolla, Missouri 65409, USA*

[3]*Department of Physics, State Key Laboratory of Low-Dimensional Quantum Physics, Tsinghua University, Beijing 100084, China*

[4]*Theoretical Division, Los Alamos National Laboratory, Los Alamos, New Mexico 87545, USA*

(Received 18 November 2016; published 2 February 2017)

We report a combined experimental and theoretical study of the electron-impact ionization of water (H_2O) at the relatively low incident energy of $E_0 = 81$ eV in which either the $1b_1$ or $3a_1$ orbitals are ionized leading to the stable H_2O^+ cation. The experimental data were measured by using a reaction microscope, which can cover nearly the entire 4π solid angle for the secondary electron emission over a range of ejection energies. We present experimental data for the scattering angles of 6° and 10° for the faster of the two outgoing electrons as a function of the detection angle of the secondary electron with energies of 5 and 10 eV. The experimental triple-differential cross sections are internormalized across the measured scattering angles and ejected energies. The experimental data are compared with predictions from two molecular three-body distorted-wave approaches: one applying the orientation-averaged molecular orbital (OAMO) approximation and one using a proper average (PA) over orientation-dependent cross sections. The PA calculations are in better agreement with the experimental data than the OAMO calculations for both the angular dependence and the relative magnitude of the observed cross-section structures.

DOI: 10.1103/PhysRevA.95.022701

I. INTRODUCTION

Electron-impact ionization dynamics of atoms and molecules have been of great interest from both theoretical and experimental points of view. It plays a crucial role in a variety of scientific and practical applications ranging from radiation chemistry and biology to astrophysics and atmospheric sciences [1,2]. It has been discovered recently that low-energy electrons can significantly induce breaks in DNA strands via the dissociative electron attachment resonances and a superposition of various nonresonant mechanisms related to excitation dissociation and ionization processes [3,4].

The water molecule (H_2O) is important in this respect, since it is ubiquitous on earth and surrounds all biological matter. Understanding the ionization dynamics requires a detailed knowledge of the interaction probabilities (i.e., the cross sections). A comprehensive way of characterizing the electron-impact ionization dynamics is to detect the two outgoing electrons in coincidence, the so-called $(e,2e)$ studies [5,6], which determine the momentum vectors of all final-state particles. The quantity measured in the $(e, 2e)$ experiments is the triple-differential cross section (TDCS), i.e., a cross section that is differential in the solid angles of both electrons and the energy of one of them. The energy of the other electron is given by energy conservation [7,8]. Such kinematically complete experiments serve as a powerful tool to comprehensively test theoretical models that account for the quantum few-body dynamics which are important to aid in the development of theoretical models and to provide the input parameters in Monte Carlo simulations in medical radiation therapy.

In recent years, theory has made tremendous progress in describing the electron-impact ionization dynamics of simple atoms and molecules; see, e.g., Refs. [9–17]. Much more challenging, however, is the treatment of more complex targets, like heavy atoms and molecules. Electron-impact ionization dynamics of the water molecule has been previously studied by the Lohmann group in the coplanar asymmetric geometry at $E_0 = 250$ eV by using a conventional $(e,2e)$ spectrometer to examine ionization of the $2a_1$, $1b_2$, $3a_1$, and $1b_1$ states of H_2O [18]. Murray and co-workers performed coplanar symmetric and asymmetric $(e,2e)$ studies for the $1b_1$ state of H_2O [19] and symmetric coplanar and noncoplanar studies for the $3a_1$ state of H_2O at low impact energies [20]. Several models have been developed to describe the ionization dynamics of H_2O. The agreement between theories and experiments, however, is not as good as results for the ionization of simple targets; see, e.g., Refs. [18–26]. Recent calculation of $(e,2e)$ on CH_4 using the molecular three-body distorted-wave approximation found that the method with proper averages (PA) is in much better agreement with experiment than the orientation-averaged molecular orbitals (OAMO) calculations [27]. On the other hand, experimental techniques were recently developed that allow for simultaneously accessing a large fraction of the entire solid angle and a large range of energies of the continuum electrons in the final state [28,29], the entire angular acceptance for the slow ejected electron within the scattering plane [30] and, more recently, the measurements of internormalized cross sections [13,31,32]. Thus, theories can be tested significantly more comprehensively over a large range of the final-state phase space.

In the present work, we perform a kinematically complete study of electron-impact ionization of H_2O at low projectile energy ($E_0 = 81$ eV). Ionization of either the $1b_1$ or $3a_1$ orbitals is observed (we do not resolve the individual states) where the residual ion is stable and does not dissociate:

$$e_0 + H_2O \rightarrow H_2O^+ + e_1 + e_2. \quad (1)$$

The TDCSs were measured by covering a large part of the full solid angle for the emitted electron. Since the experimental data are internormalized for different kinematical situations, a single common scaling factor is sufficient to fix the absolute value of all the experimental data which then can be compared with the theoretical predictions. The measurements reported here cover two ejected-electron energies ($E_2 = 5.0$ and 10.0 eV) and two projectile scattering angles ($\theta_1 = 6^\circ$ and 10.0°). The experimental data are compared with theoretical predictions from two different versions of the molecular three-body distorted-wave approximation (M3DW). While both include the final-state postcollision interaction (PCI) exactly, they treat the averaging over spatial molecular alignment with different degrees of sophistication [27].

This paper is organized as follows: After a brief description of the experimental apparatus in Sec. II, we summarize the essential points of the two theoretical models in Sec. III. The results are presented and discussed in Sec. IV, before we finish with the conclusions in Sec. V. Unless specified otherwise, atomic units (a.u.) are used throughout.

II. EXPERIMENTAL METHOD

The experiment was performed by using a reaction microscope [28] that was specially built for electron-impact ionization studies. It was recently updated with a pulsed photoemission electron gun [33,34]. Since details of the experimental setup can be found in Refs. [28,33,34], only a brief outline will be given here. The well-focused ($\approx$1 mm diameter), pulsed electron beam with an energy of $E_0 = 81$ eV is crossed with a continuous supersonic gas jet, which is produced by using a 30 μm nozzle and two-stage supersonic gas expansion. Here, helium gas was used with a partial pressure of 1 bar mixed with water vapor with a partial pressure of about 400 mbar. The electron beam is generated by illuminating a tantalum photocathode with a pulsed ultraviolet laser beam ($\lambda = 266$ nm, $\Delta t < 0.5$ ns). The energy and temporal width of the electron pulses are about 0.5 eV (ΔE_0) and 0.5 ns (Δt_0), respectively.

Homogeneous magnetic and electric fields guide electrons and ions from the reaction volume onto two position- and time-sensitive microchannel plate detectors that are equipped with fast multihit delay-line readout. The projectile beam axis (defining the longitudinal z direction) is aligned parallel to the electric and magnetic extraction fields. Therefore, after crossing the target gas jet, the unscattered primary beam reaches the center of the electron detector, where a central bore in the multichannel plates allows it to pass without inducing a signal. The detection solid angle for H_2O^+ ions is 4π. The acceptance angle for detection of electrons up to an energy of 15 eV is also close to 4π, except for the acceptance holes at small forward and backward angles where the electrons end up in the detector bore.

Experimental data are recorded by triple-coincidence detection of two electrons (e_1 and e_2) and the H_2O^+ cation. The three-dimensional momentum vectors and, consequently, kinetic energies and emission angles of final-state electrons and ions are determined from the individually measured time-of-flight and position of particles hitting the detectors. The electron binding energy ($\varepsilon_B = E_0 - E_1 - E_2$) resolution of $\Delta\varepsilon_B \approx 2.5$ eV has been obtained in the present experiment. Since the complete experimentally accessible phase space is measured simultaneously, all relative data are cross-normalized and only a single global factor fixing the absolute scale is required in comparison of theory and experiment [13,31,32].

III. THEORETICAL MODELS

We used two theoretical methods to describe the present electron-impact ionization process. Although they have been described previously [35–38] we summarize the essential ideas and the particular ingredients for the current cases of interest in order to make this paper self-contained. More detailed information can be found in the references given. The direct-scattering amplitude is given by

$$T_{\rm dir} = \underbrace{\langle \chi_a^-(\boldsymbol{k}_a,\boldsymbol{r}_0)\chi_b^-(\boldsymbol{k}_b,\boldsymbol{r}_1)C_{ab}(\boldsymbol{r}_{01})}_{\text{Final State}} \times |W| \underbrace{\phi_{Dy}(\boldsymbol{r}_1,\boldsymbol{R})\chi_i^+(\boldsymbol{k}_i,\boldsymbol{r}_0)\rangle}_{\text{Initial State}}, \quad (2)$$

where $\boldsymbol{k}_i$, $\boldsymbol{k}_a$, and $\boldsymbol{k}_b$ are the wave vectors for the initial, scattered, and ejected electrons, respectively, $\chi_i^+(\boldsymbol{k}_i,\boldsymbol{r}_0)$ is an initial-state continuum distorted wave and the (+) indicates outgoing-wave boundary conditions, $\chi_a^-(\boldsymbol{k}_a,\boldsymbol{r}_0)$, $\chi_b^-(\boldsymbol{k}_b,\boldsymbol{r}_1)$ are the scattered and ejected-electron distorted waves with incoming-wave boundary conditions, and the factor $C_{ab}(\boldsymbol{r}_{01})$ is the final-state Coulomb-distortion factor between the two electrons normally called the postcollision interaction (PCI). Here we use the exact final-state electron-electron interaction and not an approximation for it such as the Ward–Macek factor [39]. The perturbation $W = V_i - U_i$, where V_i is the initial-state interaction potential between the incident electron and the neutral molecule, and U_i represents the spherically symmetric interaction between the projectile and the active electron which is used to calculate the initial-state distorted wave $\chi_i^+(\boldsymbol{k}_i,\boldsymbol{r}_0)$. Here $\phi_{Dy}(\boldsymbol{r}_1,\boldsymbol{R})$ is the initial bound-state wave function, which is commonly called the Dyson molecular orbital, for the active electron and it depends both on $\boldsymbol{r_1}$ and on the orientation of the molecule which is designated by $\boldsymbol{R}$. The triple-differential cross section (TDCS) for a given orientation $\boldsymbol{R}$ with respect to the laboratory frame can be obtained from

$$\sigma^{\rm TDCS}(\boldsymbol{R}) = \frac{1}{(2\pi)^5}\frac{k_a k_b}{k_i}[|T_{\rm dir}(\boldsymbol{R})|^2 + |T_{\rm exc}(\boldsymbol{R})|^2 + |T_{\rm dir}(\boldsymbol{R}) - T_{\rm exc}(\boldsymbol{R})|^2], \quad (3)$$

where the exchange-scattering $T_{\rm exc}$ is calculated similarly to $T_{\rm dir}$ except that the particles 1 and 2 are interchanged in the final-state wave function. To take the proper average (PA) over all molecular orientations [37], the TDCS is calculated for each orientation and then averaged over all possible orientations so that

$$\sigma^{PA} = \frac{\int \sigma^{\rm TDCS}(\boldsymbol{R})d\Omega_R}{\int d\Omega_R}. \quad (4)$$

The only term in the integral for the T matrix that depends on the orientation is the Dyson wave function. In the orientation averaged molecular orbital (OAMO) approximation [35], we

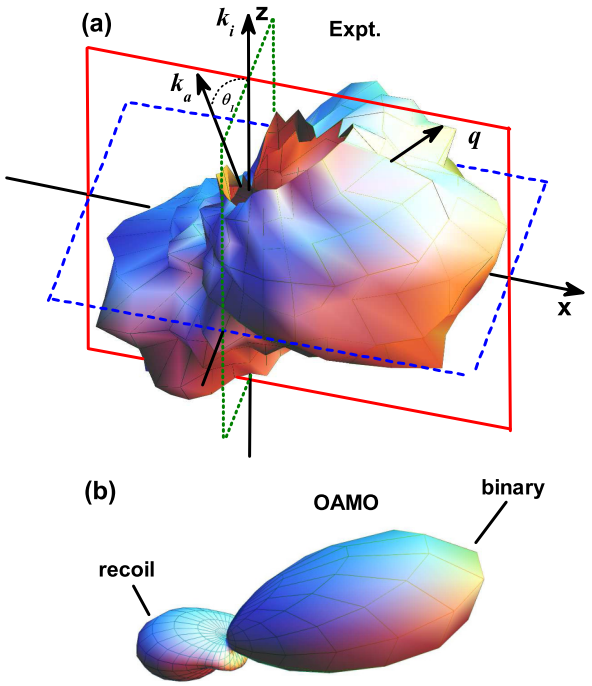

FIG. 1. Summed TDCS for experiment (top panel) and OAMO theory (bottom panel) presented as 3D images for electron-impact ($E_0 = 81$ eV) ionization of $1b_1$ and $3a_1$ orbitals of H_2O. The scattering angle is $\theta_1 = -10^\circ$, and the ejected-electron energy is $E_2 = 10$ eV. The experimental and theoretical data are normalized to unity for the binary peaks.

average the wave function over all orientations and then we calculate a single TDCS. This approximation saves a lot of computer time since the PA needs thousands of processors to do a single calculation whereas the OAMO needs less than hundred.

IV. RESULTS AND DISCUSSION

Water (H_2O) contains 10 electrons and has five molecular orbitals: $1a_1$, $2a_1$, $1b_2$, $3a_1$ and $1b_1$. The reported valence electron binding energies of water monomer are 32.4, 18.7, 14.8, and 12.6 eV corresponding to the $(2a_1)^{-1}$, $(1b_2)^{-1}$, $(3a_1)^{-1}$, and $(1b_1)^{-1}$ states, [40], respectively. We study electron-impact ionization of H_2O with the formation of the stable H_2O^+ cation which results from the ionization of either the $1b_1$ or $3a_1$ orbitals. In the present experiment the $1b_1$ and $3a_1$ orbitals are not resolved due to the limited binding-energy resolution, thus, the experimental data represent the summed TDCS for the ionization of the $1b_1$ and $3a_1$ orbitals of H_2O. Figure 1 shows the experimental and theoretical TDCS for ionization of H_2O by 81 eV electron impact as three-dimensional (3D) polar plots for a projectile scattering angle of $\theta_1 = -10^\circ$ as a function of the emission direction of a slow ejected electron with $E_2 = 10$ eV energy. Figure 1(a) corresponds to the experimental data, while Fig. 1(b) shows the calculated result from the OAMO method. The projectile enters from the bottom with momentum $\boldsymbol{k}_i$ and is scattered to the left with momentum $\boldsymbol{k}_a$ (hence the minus sign in the notation for the scattering angle). These two vectors define the scattering (xz) plane, as indicated by the solid red frame in Fig. 1(a). The momentum transferred to the target $\boldsymbol{q} = \boldsymbol{k}_i - \boldsymbol{k}_a$, is also shown on the figures.

In these 3D plots, the TDCS for a particular direction is given as the distance from the origin of the plot to the point on the surface which is intersected by the ejected electron's emission direction. The kinematics chosen displays exemplarily the principal features of the emission pattern: it is governed by the well-known binary and recoil lobes. The binary lobe is oriented roughly along the direction of the momentum transfer $\boldsymbol{q}$, which would correspond to electrons emitted after a single binary collision with the projectile. In the opposite direction the recoil lobe is found, where the outgoing slow electron, initially moving in the binary direction, additionally backscatters in the ionic potential. For ionization from p orbitals, the binary peak often exhibits a minimum along the momentum transfer direction and there is a small minimum seen in the experimental data. This is the result of the characteristic momentum profile of the p-like $1b_1$ and $3a_1$ orbitals of H_2O that has a node for vanishing momentum [40]. The experimental and theoretical 3D plots are normalized to unity for the binary peaks. We see that the theoretical recoil peak is too small and the size of the out-of-scattering-plane cross section is strongly underestimated by OAMO theory. Furthermore, the minimum along the momentum transfer direction indicated in the experimental pattern is not present in the theoretical result. For the PA calculation no full 3D image was obtained since this theory is orders of magnitude computationally more expensive and so calculations were restricted to major cutting planes which are discussed in the following. However, the PA approach does predict a minimum similar to the experimental data.

For a quantitative comparison between experiment and both the OAMO and PA methods, the cross sections in three orthogonal planes are presented in Figs. 2–4. These are cuts through the 3D TDCS image as indicated in Fig. 1(a) by the solid, dashed, and dotted frames. The experimental data represent the summed TDCS for the ionization of both the $1b_1$ and $3a_1$ orbitals of H_2O while for theories, both the summed cross sections as well as the separate $1b_1$ and $3a_1$ cross sections are shown in Figs. 2–4. The studied kinematical conditions correspond to projectile scattering angles of $\theta_1 = -6^\circ$ and -10°, and to ejected-electron energies of $E_2 = 5$ eV and 10 eV, respectively. The scaling factor used to normalize the experimental data to the theories was found by achieving a good visual fit of experiment and the PA calculations for the TDCS in the scattering plane at $\theta_1 = -10^\circ$ and $E_2 = 10$ eV [Fig. 2(h)]. This factor was subsequently applied to all other kinematics and planes, i.e., the experimental data are consistently cross normalized to each other. The OAMO theoretical results are multiplied by a factor of ten in order to compare with the results from experiment and PA calculations.

Figure 2 shows the results for detection of the secondary electron in the scattering plane, i.e., the xz plane of Fig. 1(a). It is obvious that, for the TDCS summed over $1b_1$ and $3a_1$ orbitals, the OAMO strongly overestimates the size of the binary peak relative to the recoil peak. While both theories predict a double binary peak for all four cases, the PA calculations have a broader double binary peak with a

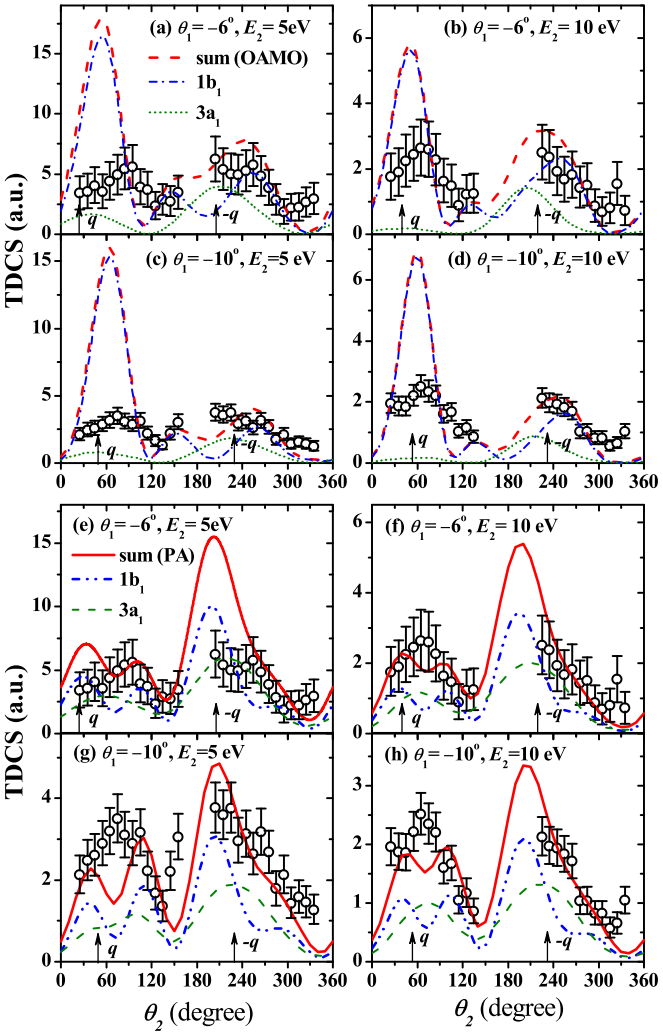

FIG. 2. Experimental and theoretical triple-differential cross sections (TDCS) for electron-impact ($E_0 = 81$ eV) ionization of $1b_1$ and $3a_1$ orbitals of H_2O presented as a function of the ejected-electron (e_2) emission angle at scattering angles $\theta_1 = -6°$ and $\theta_1 = -10°$ for ejected-electron energies $E_2 = 5$ eV (left column) and $E_2 = 10$ eV (right column). Experimental data (open circles with error bars) are the summed TDCS and theoretical calculations (lines) for the summed and the separate $1b_1$ and $3a_1$ TDCS are obtained by OAMO (top two rows) and PA (bottom two rows) methods. The vertical arrows indicate the momentum transfer direction q and its opposite $-q$. The results are for the scattering plane, i.e., the xz plane of Fig. 1(a).

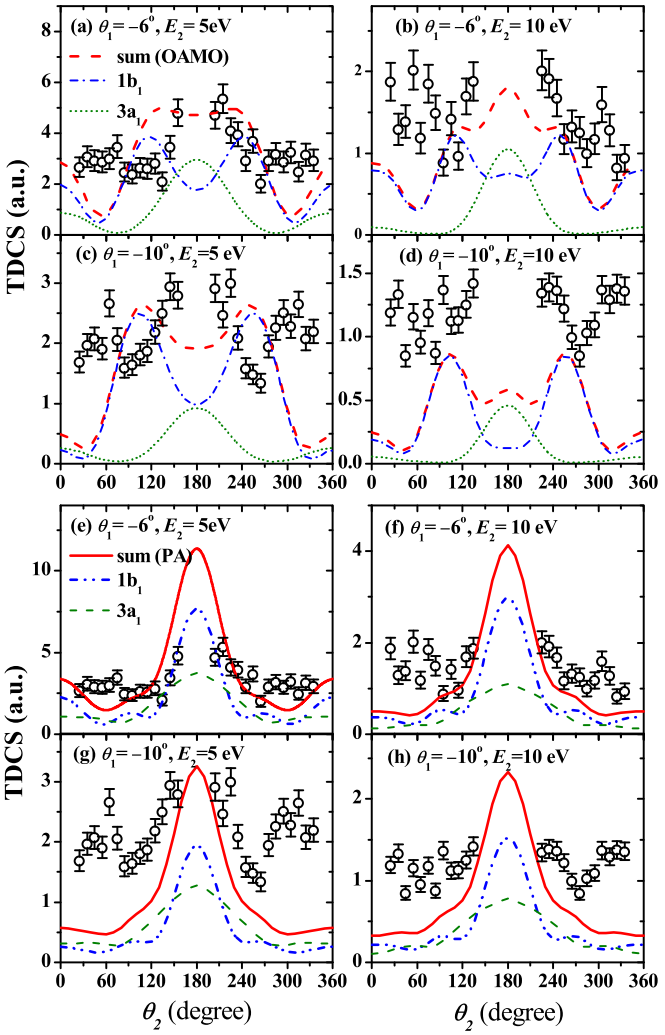

FIG. 3. Same as Fig. 2 for the "half-perpendicular" plane, i.e., the yz plane of Fig. 1(a).

minimum near the momentum transfer direction which is in better agreement with experiment. For the OAMO results, the second peak is much smaller and shifted to much larger angles. In experiment, the minimum in the binary lobe is not observed except for the case of $\theta_1 = -10°$ and $E_2 = 10$ eV where a minimum is hinted at about the momentum transfer direction. While both the OAMO and PA results predict a single peak structure for the recoil lobe, PA predicts a shoulder at the large angle side consistent with the experimental data. Although the cross section close to 180° cannot be accessed experimentally, the available data suggest a very broad recoil peak similar to PA especially for $\theta_1 = -10°$ and $E_2 = 5$ eV. Overall, regarding the relative angular dependence of the TDCSs, the PA is in much better agreement with experiment than the OAMO.

It can be seen in Fig. 2 that the two theories differ strongly from each other, especially for the separate $1b_1$ calculations. The OAMO TDCS for ionization of the $1b_1$ orbital shows a much stronger binary peak than recoil peak while the PA results exhibit a stronger recoil peak than binary peak, consistent with the experimental data. Both the OAMO and PA results have double binary peaks with minimum shifted to larger angles than the momentum transfer direction. However, the OAMO minimum is shifted to much larger angles and the PA minimum is closer to experiment for the cases where experiment sees a double binary peak. On the other side, the predicted patterns for $3a_1$ are rather similar between OAMO and PA with a small binary peak and larger recoil peak.

Figure 3 shows a comparison between experiment and theory for the yz plane (half-perpendicular plane). For this plane, symmetry considerations require the cross sections to be symmetric about 180°, which can indeed be seen in both theory and experiment. In experiment, there is an indication of a three-lobe structure for all the cases. It can be seen in the 3D plot of Fig. 1(a) that this plane cuts through the

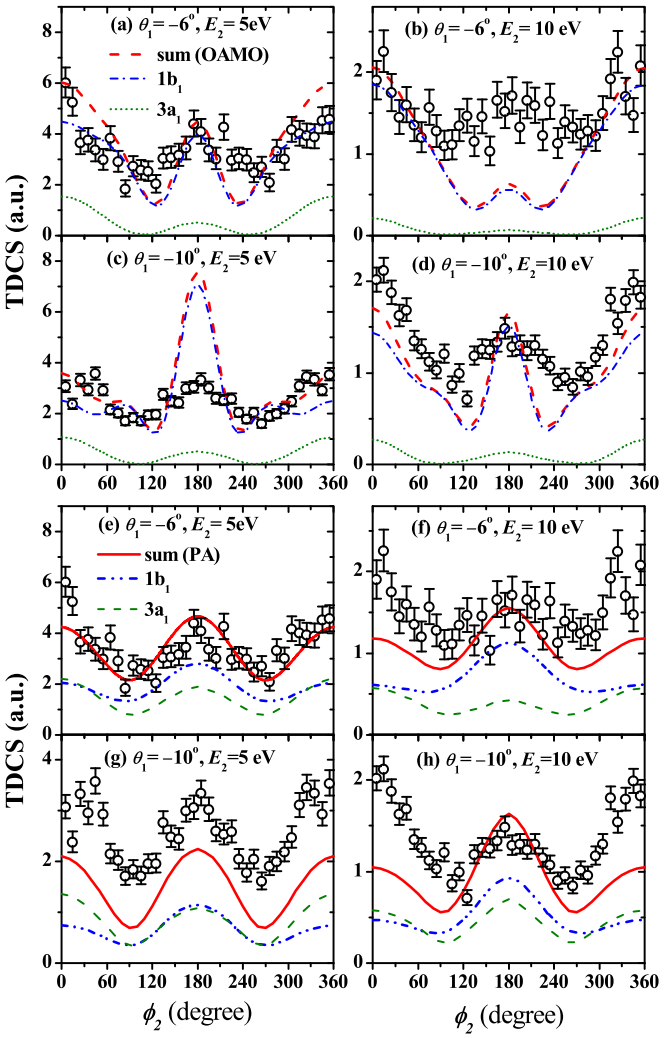

FIG. 4. Same as Fig. 2 for the "full-perpendicular" plane, i.e., the xy plane of Fig. 1(a).

binary peak which results in two symmetric maxima in the ranges $\theta_2 = 30°$–$90°$ and $\theta_2 = 270°$–$330°$, respectively. In addition, the recoil lobe gives rise to the central maximum at $\theta_2 = 180°$. Concerning the central peaks, the PA is in much better agreement with experiment than the OAMO. Here, the OAMO predicts a minimum or a flat distribution at $\theta_2 = 180°$ except for the case of $\theta_1 = -6°$ for $E_2 = 10$ eV. In all panels, the predicted cross sections of OAMO are significantly smaller than observed experimentally for $\theta_2 \leqslant 90°$ and, by symmetry, for $\theta_2 \geqslant 270°$. The PA predictions also underestimate the cross section in this angular region except for $\theta_1 = -6°$, $E_2 = 5$ eV [Fig. 3(e)] where the agreement with experiment is rather good. Theories underestimate the out-of-scattering-plane size of the binary lobes. It is again interesting to note that significant discrepancies are seen between OAMO and PA in particular for the separate $1b_1$ calculations where the OAMO exhibits a minimum at $\theta_2 = 180°$ with two maxima at about 120° and 240° while the PA predicts a strong maximum at $\theta_2 = 180°$ with two side peaks at about 90° and 270°. The calculations for $3a_1$ are again rather similar between OAMO and PA.

Figure 4 shows the comparison between experiment and theories for the full-perpendicular plane (i.e., the xy plane). Here, the experimental angular acceptance covers the entire 0°–360° range, but the cross sections are again symmetric with respect to 180°. The binary and recoil peaks are observed in the vicinity of $\phi_2 = 0°$ and 180°, respectively. The two theories in this case agree rather well in shape for the summed and the separate $1b_1$ and $3a_1$ TDCS, and they are in rather good agreement with the experimental data, except that the relative intensity of the recoil peaks are too low for Fig. 4(b) and too high for Fig. 4(c) in the OAMO curves.

V. CONCLUSIONS

We have reported a comprehensive study of the electron-impact ionization dynamics of H_2O for a projectile energy of 81 eV. Experimentally, the three-dimensional momentum vectors of the final-state particles are determined for a large part of the solid angle for the slow emitted electron. Thus, full three-dimensional representations of the cross sections are accessible. The summed triple-differential cross sections for ionization of $1b_1$ and $3a_1$ orbitals of H_2O obtained experimentally were internormalized across the scattering angles $\theta_1 = -6°$ and $-10°$ and ejected-electron energies $E_2 = 5$ and 10 eV, thus providing a thorough test for the theoretical models. The experimental data were compared with predictions from the molecular three-body distorted-wave approximation coupled with OAMO and PA methods.

There is overall much better agreement between the PA predictions and the experimental data than the OAMO concerning both the angular dependence of the cross sections and the relative magnitude over the entire range of angle and energy conditions analyzed. Noticeable systematic discrepancies occur in the half-perpendicular plane (Fig. 3), where both OAMO and PA predictions are significantly smaller than that observed experimentally in the angular ranges $\theta_2 \leqslant 90°$ and, by symmetry, $\theta_2 \geqslant 270°$. In comparison for ionization of the atomic target Ne, which has the same number of bound electrons as H_2O, the three-body distorted-wave theory reveals an unprecedented degree of agreement with experiment [13,31]. The two calculations based on the three-body distorted-wave theory differ strongly from each other in both the relative shape and the magnitude of the cross sections. This illustrates the fact that the theoretical treatment of electron-impact ionization of molecules is more complicated and the results are very sensitive to the details of the model employed. The fact that the PA calculation agrees better with experiment for the scattering plane than the other two planes suggests that second Born terms which are not included in the present treatment may be more important in the out-of-the scattering plane than in the scattering plane. The present work indicates that it is more accurate to perform a proper average over orientation-dependent cross sections than to use the orientation-averaged molecular orbital for calculations. The computational cost of the proper average method, however, is much higher than the orientation-averaged molecular orbital approximation. OAMO calculations can be easily performed by using less than 100 processors while PA calculations require several thousand processors!

ACKNOWLEDGMENTS

This work was supported, in part, by the United States National Science Foundation under Grant No. PHY-1505819 (S.A., E.A., and D.M.) and by the National Natural Science Foundation of China under Grant No. 11174175 (C.N.). Computational work was performed with Institutional Computing resources made available through the Los Alamos National Laboratory. The Los Alamos National Laboratory is operated by Los Alamos National Security, LLC, for the National Nuclear Security Administration of the US Department of Energy under Contract No. DE-AC5206NA25396. S.A. and E.A. would also like to thank the Libyan Ministry of Higher Education's scholarship for financial support.

[1] E. Alizadeh, T. M. Orlando, and L. Sanche, Annu. Rev. Phys. Chem. **66**, 379 (2015).

[2] B. C. Garrett, D. A. Dixon, D. M. Camaioni, D. M. Chipman, M. A. Johnson, C. D. Jonah, G. A. Kimmel, J. H. Miller, T. N. Rescigno, P. J. Rossky, S. S. Xantheas, S. D. Colson, A. H. Laufer, D. Ray, P. F. Barbara, D. M. Bartels, K. H. Becker, K. H. Bowen, S. E. Bradforth, I. Carmichael, J. V. Coe, L. R. Corrales, J. P. Cowin, M. Dupuis, K. B. Eisenthal, J. A. Franz, M. S. Gutowski, K. D. Jordan, B. D. Kay, J. A. LaVerne, S. V. Lymar, T. E. Madey, C. W. McCurdy, D. Meisel, S. Mukamel, A. R. Nilsson, T. M. Orlando, N. G. Petrik, S. M. Pimblott, J. R. Rustad, G. K. Schenter, S. J. Singer, A. Tokmakoff, L.-S. Wang, and T. S. Zwier, Chem. Rev. (Washington, DC, USA) **105**, 355 (2005).

[3] M. A. Huels, B. Boudaiffa, P. Cloutier, D. Hunting, and L. Sanche, J. Am. Chem. Soc. **125**, 4467 (2003).

[4] S. M. Pimblott and J. A. LaVerne, Radiat. Phys. Chem. **76**, 1244 (2007).

[5] H. Ehrhardt, M. Schulz, T. Tekaat, and K. Willmann, Phys. Rev. Lett. **22**, 89 (1969).

[6] U. Amaldi, A. Egidi, R. Marconero, and G. Pizzella, Rev. Sci. Instrum. **40**, 1001 (1969).

[7] H. Ehrhardt, K. Jung, G. Knoth, and P. Schlemmer, Z. Phys. D: At., Mol. Clusters **1**, 3 (1986).

[8] A. Lahmam-Bennani, J. Phys. B: At., Mol. Opt. Phys. **24**, 2401 (1991).

[9] T. N. Rescigno, M. Baertschy, W. Isaacs, and C. McCurdy, Science **286**, 2474 (1999).

[10] I. Bray, D. Fursa, A. Kadyrov, A. Stelbovics, A. Kheifets, and A. Mukhamedzhanov, Phys. Rep. **520**, 135 (2012).

[11] X. Ren, A. Senftleben, T. Pflüger, K. Bartschat, O. Zatsarinny, J. Berakdar, J. Colgan, M. S. Pindzola, I. Bray, D. V. Fursa, and A. Dorn, Phys. Rev. A **92**, 052707 (2015).

[12] O. Zatsarinny and K. Bartschat, Phys. Rev. Lett. **107**, 023203 (2011).

[13] T. Pflüger, O. Zatsarinny, K. Bartschat, A. Senftleben, X. Ren, J. Ullrich, and A. Dorn, Phys. Rev. Lett. **110**, 153202 (2013).

[14] X. Ren, A. Senftleben, T. Pflüger, A. Dorn, J. Colgan, M. S. Pindzola, O. Al-Hagan, D. H. Madison, I. Bray, D. V. Fursa, and J. Ullrich, Phys. Rev. A **82**, 032712 (2010).

[15] O. Al-Hagan, C. Kaiser, A. J. Murray, and D. Madison, Nat. Phys. **5**, 59 (2009).

[16] X. Ren, T. Pflüger, S. Xu, J. Colgan, M. S. Pindzola, A. Senftleben, J. Ullrich, and A. Dorn, Phys. Rev. Lett. **109**, 123202 (2012).

[17] M. C. Zammit, J. S. Savage, D. V. Fursa, and I. Bray, Phys. Rev. Lett. **116**, 233201 (2016).

[18] D. S. Milne-Brownlie, S. J. Cavanagh, B. Lohmann, C. Champion, P. A. Hervieux, and J. Hanssen, Phys. Rev. A **69**, 032701 (2004).

[19] C. Kaiser, D. Spieker, J. Gao, M. Hussey, A. Murray, and D. H. Madison, J. Phys. B: At., Mol. Opt. Phys. **40**, 2563 (2007).

[20] K. L. Nixon, A. J. Murray, O. Al-Hagan, D. H. Madison, and C. Ning, J. Phys. B: At., Mol. Opt. Phys. **43**, 035201 (2010).

[21] C. Champion, C. Dal Cappello, S. Houamer, and A. Mansouri, Phys. Rev. A **73**, 012717 (2006).

[22] C. Dal Cappello, Z. Rezkallah, S. Houamer, I. Charpentier, P. A. Hervieux, M. F. Ruiz-Lopez, R. Dey, and A. C. Roy, Phys. Rev. A **84**, 032711 (2011).

[23] I. Tóth, R. I. Campeanu, and L. Nagy, Eur. Phys. J. D **66**, 1 (2012).

[24] M. Sahlaoui, M. Bouamoud, B. Lasri, and M. Dogan, J. Phys. B: At., Mol. Opt. Phys. **46**, 115206 (2013).

[25] C.-Y. Lin, C. W. McCurdy, and T. N. Rescigno, Phys. Rev. A **89**, 012703 (2014).

[26] S. B. Zhang, X. Y. Li, J. G. Wang, Y. Z. Qu, and X. Chen, Phys. Rev. A **89**, 052711 (2014).

[27] H. Chaluvadi, C. G. Ning, and D. Madison, Phys. Rev. A **89**, 062712 (2014).

[28] J. Ullrich, R. Moshammer, A. Dorn, R. Dörner, L. Schmidt, and H. Schmidt-Böcking, Rep. Prog. Phys. **66**, 1463 (2003).

[29] M. Dürr, C. Dimopoulou, A. Dorn, B. Najjari, I. Bray, D. V. Fursa, Z. Chen, D. H. Madison, K. Bartschat, and J. Ullrich, J. Phys. B: At., Mol. Opt. Phys. **39**, 4097 (2006).

[30] M. A. Stevenson and B. Lohmann, Phys. Rev. A **77**, 032708 (2008).

[31] X. Ren, S. Amami, O. Zatsarinny, T. Pflüger, M. Weyland, W. Y. Baek, H. Rabus, K. Bartschat, D. Madison, and A. Dorn, Phys. Rev. A **91**, 032707 (2015).

[32] X. Ren, S. Amami, O. Zatsarinny, T. Pflüger, M. Weyland, A. Dorn, D. Madison, and K. Bartschat, Phys. Rev. A **93**, 062704 (2016).

[33] X. Ren, T. Pflüger, M. Weyland, W. Y. Baek, H. Rabus, J. Ullrich, and A. Dorn, J. Chem. Phys. **141**, 134314 (2014).

[34] X. Ren, E. Jabbour Al Maalouf, A. Dorn, and S. Denifl, Nat. Commun. **7**, 11093 (2016).

[35] J. Gao, J. L. Peacher, and D. H. Madison, J. Chem. Phys. **123**, 204302 (2005).

[36] D. H. Madison and O. Al-Hagan, J. At. Mol. Opt. Phys. **2010**, 24 (2010).

[37] E. Ali, K. Nixon, A. Murray, C. Ning, J. Colgan, and D. Madison, Phys. Rev. A **92**, 042711 (2015).

[38] A. Sakaamini, S. Amami, A. J. Murray, C. Ning, and D. Madison, J. Phys. B: At., Mol. Opt. Phys. **49**, 195202 (2016).

[39] S. J. Ward and J. H. Macek, Phys. Rev. A **49**, 1049 (1994).

[40] Y. R. Miao, C. G. Ning, and J. K. Deng, Phys. Rev. A **83**, 062706 (2011).